coatings

MDPI

Article

Zein-Functionalized MCM-41 Silica Nanoparticles with Enzyme-Responsive for Controlled Release in Antibacterial Activity

Huimin Sun [1], Yuyang Lu [1], Jie Sheng [1,*] and Yishan Song [1,2,*]

[1] College of Food Science and Technology, Shanghai Ocean University, Shanghai 201306, China
[2] Department of Chemistry, Shanghai Ocean University, Shanghai 201306, China
* Correspondence: jsheng@shou.edu.cn (J.S.); yssong@shou.edu.cn (Y.S.)

Abstract: This research provided a novel enzyme-responsive antimicrobial carrier aiming at overcoming the volatile loss of active antibacterial components, by employing mesoporous silica nanoparticles (MCM-41) as the matrix of encapsulation and Zein as the molecular gate. Since Zein could be consumed by bacteria, Zein-functionalized MCM-41 acted as an enzyme-responsive gate and improved the controlled-release capacity. The results showed that the amount of capsaicin released from Zein-functionalized MCM-41 without bacteria was quite low compared with the essential oils liberated with bacteria. This validated that the delivery of capsaicin was hampered by Zein and the existence of *Escherichia coli* (*E. coli)* and *Staphylococcus aureus* (*S. aureus)* promoted the release of encapsulated cargo. The release rate of capsaicin in Zein-functionalized MCM-41 climbed with the growth velocity of bacteria. These functions were realized in the form of controlled diffusion of essential oils encapsulated in MCM-41 by electrostatic interaction, and Zein was performed by both covalent bonding interaction and electrostatic interaction. Zein-functionalized MCM-41 was 2.4 times more effective in killing *E. coli* and 1.2 times more effective in inhibiting *S. aureus* than an equal amount of free capsaicin, and possessed a long-lasting antibacterial activity. The responsive antimicrobial material might be used as a promising preservative in the food industry for antimicrobial activity enhancement.

Keywords: antibacterial activity; gated release; MCM-41; capsaicin; Zein

Citation: Sun, H.; Lu, Y.; Sheng, J.; Song, Y. Zein-Functionalized MCM-41 Silica Nanoparticles with Enzyme-Responsive for Controlled Release in Antibacterial Activity. *Coatings* **2023**, *13*, 57. https://doi.org/10.3390/coatings13010057

Academic Editor: Ajay Vikram Singh

Received: 14 November 2022
Revised: 20 December 2022
Accepted: 25 December 2022
Published: 28 December 2022

1. Introduction

Microbial contamination is responsible for food corruption and even foodborne diseases, ranging from gastroenteritis and intoxication, to shock or other syndromes [1]. The main pathogenic microorganism can be divided into two principal parts, namely Gram-negative bacteria (*Escherichia coli and Salmonella enterica*) and Gram-positive bacteria (*Staphylococcus aureus* and *Listeria monocytogenes*) [2], which are both the most common foodborne pathogens in daily life, resulting in death due to foodborne illness [3,4]. Depending on the statistics, unhealthy diets cause 11 million deaths, and a further 420,000 people die from consuming unsafe food annually [5–7]. Currently, three billion people fail to eat safe food, and unhealthy diets are linked to 6 of the top 10 risk factors for the global burden of disease [8]. Based on the experience from the COVID-19 pandemic, WHO will continue to work with partners with a One Health approach to keep communities safe from foodborne disease [9,10].

With the abuse of antibiotics, antimicrobial resistance (AMR) increasingly attracts public concern worldwide. The persistent failure to develop, manufacture, and distribute effective new antibiotics is further fueling the impact of AMR and threatens the communal ability to successfully treat bacterial infections [11]. WHO has announced that bacterial infection is the decisive cause of high neonatal mortality and inborn error, accounting for 23% and 15%, respectively. Although drug therapy has supplied appropriate treatment to improve the condition, AMR seems to be a huge challenge. In 2016, antimicrobial resistance

was first to be estimated as a cause of neonatal death, and multidrug-resistant pathogens accounted for about 30% of all global neonatal sepsis mortality [12]. In order to deal with the AMR threat, a global effort should be made and opportunities emerging from the COVID-19 pandemic must be grabbed, focusing on sustainable investments in research and development of novel and natural antibiotics. Accordingly, novel and natural compounds like essential oils should be selected to substitute the existing antibiotics, slowing the impact of microbial resistance.

Essential oils (EOs) are a complex natural product extracted from plants that are considered to have a safe food composition for food preservation [13,14]. Terpenes and aromatic compounds are the most common and effective substances found in Eos [15,16]. Based on previous research, EOs exhibit antimicrobial, anti-inflammatory, and analgesic effects under biological activities [17]. For instance, tea tree oil and oregano essential oil show great bactericidal activity against Gram-negative and Gram-positive bacteria [18–20]. Since they are unstable, easily decompose, and are volatile, plant essential oils fail to be developed or used to their full potential. Capsaicin is another typical example as an antibacterial EO, which is the major capsaicin present in peppers and have antimicrobial, anti-inflammatory, and antioxidant properties [21–23].

In recent years, the public has had more interest on nanotechnology due to its distinct properties and widespread applications in food or pharmaceutical industries [24]. Mesoporous silica nanoparticles (MSNs) have excellent carrier characteristics, including a high specific surface area (800–1000 m^2/g), adjustable aperture (2–5 nm), and flexible particle size (usually less than 200 nm) [25–27]. Furthermore, mesoporous MCM-41 is a typical molecular sieve mesoporous silica material with the regular and hexagonal arrangement of SiO_2 that has an enhanced specific surface area, good mechanical and thermal stability, and a governable pore size [28], possessing all the advantages of MSNs, with a synthesis method that is simple and efficient [29]. Studies have reported that loading EOs to mesoporous silica nanoparticles can improve its bioavailability, and achieve controlled release in a food area like targeted drug release [30–32].

Zein is a safe and non-toxic material with good biocompatibility and biodegradability that also can improve the efficiency of nanomaterial encapsulation of essential oil. Zein is the main form of protein storage in maize endosperm tissue, which can be used as nutrients for bacterial growth. Therefore, an enzyme-controlled release system has been proposed in this paper to better encapsulate capsaicin in mesoporous materials by using amino functionalization and Zein functionalization on the premise of encapsulating the essential oils of mesoporous silica [33,34]. In this controlled release system, Zein, as a gate, slowly dissolves when bacteria appear, and then the encapsulated essential oil releases through the enzymatic decomposition, inhibiting bacterial growth and achieving the effect of bacteriostasis and preservation.

2. Materials and Methods

2.1. Materials

Capsaicin (97%), tetraethyl orthosilicate (TEOS, 98%), aqueous ammonia (28%), cetyltrimethylammonium bromide (CTAB), aminopropyl triethoxysilane (APTES), absolute ethanol (99.8%), Zein (Macklin, China), phosphate buffer saline (PBS, 0.1 M, pH = 7.4), and glutaraldehyde (25%) were all of analytical grade and provided by Sangon Biotech (Shanghai, China).

2.2. Preparing Antimicrobial Supports: Preparation of NH_2-MCM-41 (NH_2/M41)

NH_2-MCM-41 was prepared by the following steps. Deionized water was mixed well with ammonia solution and CTAB was added and stirring together with the solution in a 500 mL beaker for an hour. The solution was heated to 60 °C in an oil bath by a magnetic agitator. Once CTAB was evenly dissolved, TEOS was added into the sample dropwise and stirring continued. One hour later, APTES was added dropwise with continuous mixing for 6 h. The liquid was then transferred to a stainless-steel crystallization kettle lined with polytetrafluoroethylene and let stand for 24 h at 33 °C to begin crystallizing. The solution

was washed with absolute ethanol and then centrifugations were performed for 20 min at 10,000 rpm. After the separation of the precipitate and supernatant, the supernatant was rejected and the precipitate was kept for further abstersion. Filtration and washing steps were replicated in triplicate at least three times in brine to remove the surfactant template as much as possible. The white precipitation was collected and dried at 60 °C in a vacuum oven. Using 200 mL of 99.8% pure ethanol as the extraction solvent, soxhlet extraction was used to remove the templates from the dried powder over the course of 72 h. The powder was dried in a vacuum oven at 60 °C to obtain NH_2/M41 mesoporous silica microspheres.

2.3. Preparation of Capsaicin-NH_2-MCM-41 (CAP@ NH_2/M41)

The encapsulation method here referenced previous reported methods [28]. An amount of 500 mg of particles (NH_2/M41) was transferred into a round-bottomed flask under N_2 protection. Then, 30 mL absolute ethyl alcohol and 500 mg of capsaicin were added and stirred for 24 h to optimize the embedding level in scaffolding pores of NH_2/M41.

2.4. Preparation of Zein-Capsaicin-NH_2-MCM-41 (CAP@ Zein/M41)

An amount of 500 mg of Zein was dissolved to a solution of ethyl alcohol (80%, 20 mL in 25 mL of H_2O) and mixed well. When the Zein solution was clarified and appeared faint yellow, an equal mass of CAP@ NH_2/M41 was added and the mixture was stirred at room temperature for 24 h. The final solid was gathered through filtration and washed more than three times with ethanol. Finally, the Zein protein-functionalized sample (CAP@ Zein/M41) was left to dry under room temperature (around 26 °C) (Scheme 1).

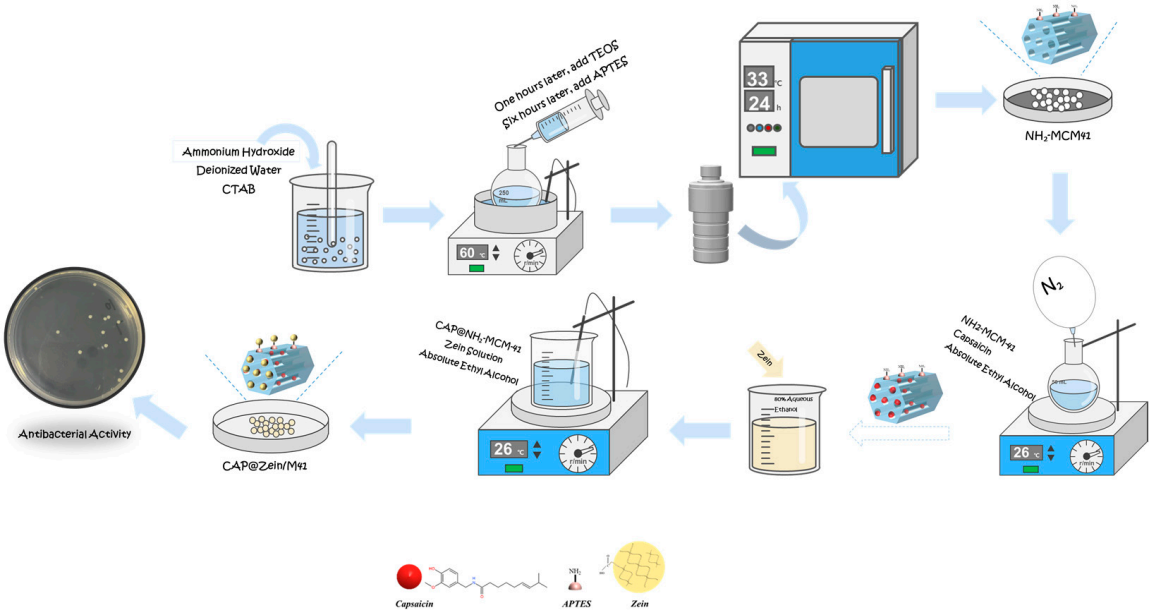

Scheme 1. Synthetic process of CAP@ Zein/M41.

2.5. Characterization of CAP@ Zein/M41

2.5.1. Scanning Electron Microscope (SEM)

The surface morphology of NH_2/M41 and CAP@ Zein/M41 was observed using a field scanning electron microscope (Hitachi SU5000, Tokyo, Japan) at an accelerating voltage of 5.0 kV. Samples were coated with platinum before observation.

2.5.2. Fourier Transform Infrared Spectroscopy (FTIR)

The FTIR spectra of these samples were calculated by a FTIR spectrometer (Nicolet Instrument, Thermo Fisher, Waltham, MA, USA). In short, each sample was mingled with moderate potassium bromide (KBr) after an accurate measurement of the amount, and then the mixture was detected using a direct compression method [35]. The spectra were

collected at a step of 4 cm^{-1} resolution within the range of 400–4000 cm^{-1} wavenumber while the baseline was corrected and converted into absorbance mode.

2.5.3. Thermogravimetric Analysis (TGA)

TGA was carried out using the synchronous thermal analysis (STA449C/4/G, Netzsch, Selb, Germany). Samples of 10 mg were placed in alumina pans, and an empty alumina pan was used as a reference. Heating was controlled by rotating the temperature up to 800 °C in 80 mL/min flows of air. The heating rate was set at 10 °C/min.

2.5.4. Particle Size and Zeta Potential

The particle size and ζ-potential of the particles were determined using a zeta-potential analyzer (Zetasizer Nano ZS90, Malvern Instruments, Malvern, UK). Measurements were set at room temperature (25 °C), with each sizing determination performed in triplicate and an average particle size expressed as the mean diameter [36].

2.5.5. Nitrogen Adsorption/Desorption

BET Nitrogen adsorption-desorption isotherms for samples were obtained using BELSORP-mini II (Bel, Bengaluru, India), where the specific surface area, volume, and pore diameter were measured [37].

2.6. Measurement of Capsaicin Release by High-Performance Liquid Chromatography (HPLC)

Both CAP@MCM-41 and CAP@ Zein/M41 were added simultaneously into 10 mL of tryptone soybean broth (TSB), where the density of *E. coli* was 10^6 CFU/mL. In parallel, CAP@ Zein/M41 was added into pure TSB solution without bacteria as the blank-controlled trial. All three experimental groups were cultured in a shaker at 180 rpm at 37 °C. Samples were made more than four times in the first one hour, and then were sampled at least two-hour intervals. Afterward, capsaicin content was measured by high-performance liquid chromatography (HPLC, Waters Technologies, Milford, MA, USA).

The capsaicin was quantified using HPLC (Waters Technologies, Milford, MA, USA), modified by a previous study [38]. An amount of 1 mL volume of solution was absorbed from three different experimental test tubes, respectively, and all filtered through 0.22 μm filters for HPLC analysis. A Zorbax SB-C18 column (250 mm × 4.6 mm, 5 μm particle size, Waters SunFire®) was used as an analytical column and was maintained at 30 °C in the column oven. The mixture of methyl alcohol and ultrapure water was used as the mobile phase and the flow rate was 1.0 mL/min. The injection volume was 10 μL and UV detection (Waters 2489 UV/Vis Detector) was performed at 280 nm. The external standard method was used for quantitative analysis.

2.7. Antibacterial Performance

2.7.1. Strains and Growth Conditions

All strains used in this study (*Escherichia coli* (*E. coli*) ATCC 25992 and *Staphylococcus aureus* (*S. aureus*) ATCC 25923) were provided by Shanghai Ocean University, China. Before experiments, from frozen stocks, strains were cultivated overnight under the appropriate growth conditions and passaged once before use. For all of the experiments, single clones picked from a tryptic soy agar (TSA) plate medium were inoculated in 10 mL of tryptic soy broth (TSB) fluid medium and grown at 37 °C with 180 rpm for 24 h at a bacteria concentration to 1×10^8 CFU/mL and used for the different assays [39]. MIC measurements were obtained as a means to normalize concentration choices. OD_{600} measurements were used to determine the lowest concentration at which no growth was detected. Each test was performed in triplicate from three experiments.

2.7.2. Bactericidal Activity of Capsaicin

The MIC approach was used to assess the antibacterial activity of capsaicin, and the method of doubling dilutions was used. In a nutshell, bacterial cultures that had grown

overnight were diluted to have a bacterial concentration of roughly 1×10^6 colony forming unit (CFU)/mL. Diluted bacterial solution was combined with capsaicin doses ranging from 64 to 0.125 mg/mL in a two-fold dilution series, and the mixture was then incubated for 24 h at 37 °C to measure the OD_{600} [40]. The MIC was calculated using the lowest capsaicin concentration that prevented bacterial growth.

2.7.3. Bactericidal Activity of CAP@ Zein/M41

Different concentration gradient samples of the product were prepared by dissolving in 10.0 mL of TSB fluid medium and a test suspension of bacteria cells was added. Aiming for 1×10^6 CFU/mL of bacterium cells, the suspension was adjusted [41]. Each sample's remaining bacteria count was calculated. Samples were serially diluted from 10^1 to 10^7, and the last three dilutions were plated in duplicate on tryptone soya agar [42]. Colony-forming units per milliliter (CFU/mL) were measured following the plates' 24-hour incubation at 37 °C. Moreover, the growth curves of *E. coli* with different concentrations of CAP@ Zein/M41 were measured using an automatic microbe growth curve automatic analyzer (Bioscreen, Turku, Finland). All tests were performed in triplicate to ensure reproducibility.

2.7.4. Morphological Changes in *E. coli* and *S. aureus*

The preliminary treatment procedures of morphological change analysis in *E. coli* and *S. aureus* are listed as follows [43]: both *E. coli* and *S. aureus* were incubated for 12 h and then processed using different concentrations of CAP@ Zein/M41 at 37 °C with continuous stirring for 3 h. After incubation, the suspensions were centrifuged at 4000 g/min for 10 min and washed twice with 0.1 M phosphate buffer solution (PBS, pH 7.4). Overnight *E. coli* and *S. aureus* were fixed in 2.5% glutaraldehyde at 4 °C. After three washes with PBS, all samples were dehydrated in sequentially graded ethanol (30%, 50%, 70%, 90%, and 100%). Finally, they were sputter-coated with platinum before SEM.

2.8. Statistical Analysis

The experimental data were repeated three times in parallel. The SPSS statistical software (version 22.0, SPSS, Inc., Chicago, IL, USA) was used for data analysis and Origin 8.5 (OriginLab, Inc., Northampton, MA, USA) was used for drawing. Different letters indicate statistical differences ($p < 0.05$).

3. Results and Discussion

3.1. Characterization of CAP@ Zein/M41

3.1.1. Scanning Electron Microscope (SEM)

The morphology of the MCM-41 and its derivatives were observed by SEM. Figure 1 presented the SEM images of the MCM-41 powders before and after modification, respectively. According to the SEM results, MCM-41 presented a hexagonal prism shape with homogenous pore size distribution (Figure 1a). Although Zein and capsaicin were coated on the silica NPs' surfaces, the modified silica NPs did not alter their morphology. Similar results were reported by Ribes et al. [44] in which the immobilization of eugenol and thymol on the surface of MCM-41 did not affect the integrity of the mesoporous silica particles [45]. Moreover, Suttiruengwong et al. [46] discovered that the appearance of shapeless silica and MCM-41 particles did not change after functionalization with thymol. Without a doubt, MCM-41 has been broadly utilized owing to its tall surface range, expansive pore volume, high levels of chemical and warm steadiness, and flexible chemical modifiable surface. It has been detailed that the functionalization of MCM-41 is a feasible path to release the essential oils with an enzyme-response gate [47].

3.1.2. Fourier Transform Infrared Spectroscopy (FTIR)

As for MCM-41, the curve presented the characteristic absorption peaks, namely the Si-O-Si group at 1049.13 cm^{-1}, -OH at 3692.20 cm^{-1}, and the weak peaks at 2924 and 2856 cm^{-1}, which were attributed to asymmetric stretching of CH_2 group of CTAB and

C-H in the hexagonal prism's structure. After surface modification with capsaicin and Zein coating, several new absorption signals appeared in Figure 2. The most notable peaks in capsaicin were observed at 2925.10 cm^{-1}, due to the stretching vibration of C-H(-CH_3), and 2852.82 cm^{-1}, belonging to the C-H(-CH_2-) stretching vibration. Peaks ranging from 1291 to 1645 cm^{-1} were due to the stretching vibration of C=O(-CH_2-CO-CH_2-) and the benzene ring [46]. The results listed several peaks at respective wavenumbers (cm^{-1}) including contributions from various functional groups of Zein at 2974.87, 2872.89, and 1421.51 cm^{-1} [47–51]. Results indicated that capsaicin and Zein had been functionalized successfully. Embedding essential oils (EOs) into MSNs makes it possible to slow down the release rate, where encapsulation and covalency are essentially two forms of EOs' insertion. Hence, this research used NH_2/M41 to encapsulate capsaicin, and covalently attached Zein to the matrix in order to enhance the controlled release effect.

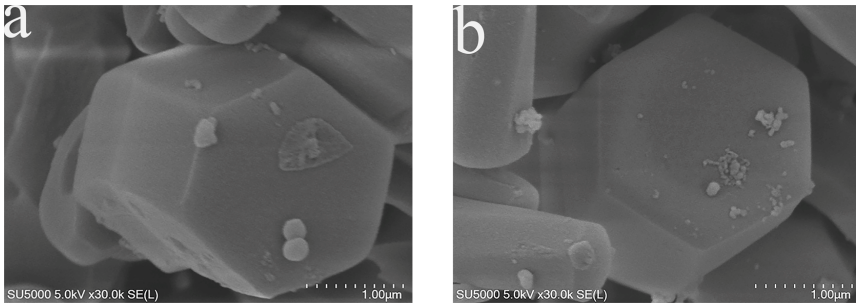

Figure 1. SEM images of (**a**) MCM-41 and (**b**) CAP@ Zein/M41.

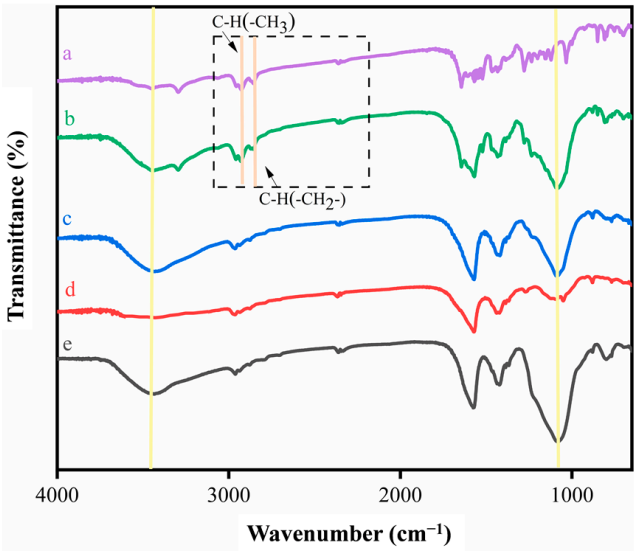

Figure 2. FT-IR spectra of (**a**) capsaicin; (**b**) CAP@ Zein/M41; (**c**) Zein/M41; (**d**) Zein and (**e**) NH_2/M41.

3.1.3. Thermogravimetric Analysis (TGA)

The thermal gravimetric analyzer (TGA) diagrams of the CAP@ Zein/M41 at each stage are shown in Figure 3. It is noticeable that almost all materials presented a similar downtrend between 35 and 180 °C, which probably resulted from the adsorbed water molecules and solvent removal from the surface layer of MCM-41, which was consistent with all other curves [52].

Furthermore, the TGA curve of MCM-41 presented only one loss point: the weight loss occurred at the temperature range of 30–100 °C due to the solvent evaporation, and that of bare CAP@MCM-41 showed a two-step one. Thus, it could be inferred that capsaicin was pyrolyzed completely since organic substances usually thermally degrade over 180 °C (Figure 3a,d) [53]. It was further marked that TGA results demonstrated the thermal

degradation of CAP@ Zein/M41 including three steps (Figure 3c,f). The first degradation step began at 30 °C due to the loss of water, with a weight loss of about less than 10%. Afterwards, the second step was accompanied with the thermal degradation of capsaicin, which was about 10% when higher than 180 °C. At temperatures above 185 °C, Zein and the remaining materials turned to ash. The thermogram suggested that the original nanoparticles could consist of around 16.9% antibacterial active ingredients, whereas the load rate of the capsaicin that was finally modified on the surface of the mesoporous silica particles was identified at 9.2%. This assured that the final product still kept the antibacterial effect through a series of modifications [54].

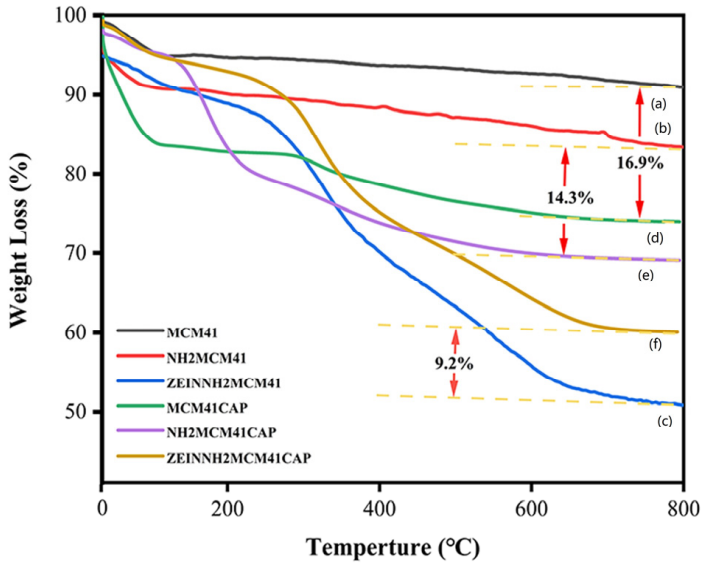

Figure 3. TGA spectra of (**a**) MCM-41; (**b**) NH_2/M41; (**c**) CAP@ Zein/M41; (**d**) CAP@M41; (**e**) CAP@ NH_2/M41; (**f**) Zein/M41.

In addition, TGA analysis was also conducted to quantify the amount of capsaicin encapsulated into NH_2/M41. The curves exhibited the remaining weight mass of capsaicin from Zein/M41. The results depicted a decent loading capacity and were in harmony with the antibacterial activity. The thermal stability of capsaicin was significantly improved by multideck functionalization, and the comparison of the final residual amount of the samples suggested the same trend. These data would be utilized in the subsequent comparison of antibacterial tests with different contents of capsaicin. Separately, amino-functionalization is an important method to enhance the stability of mesoporous silica nanoparticles [55]. (3-aminopropyl) triethoxysilane (APTES) is usually used through a novel grafting method to improve the activity, stability, and retain ability of nanoparticles [56]. Thus, ATPES was applied to further functionalize MCM-41 with amidogen, enhancing its stability and preparing for extra modification.

3.1.4. Zeta Potential

Zeta-potential analysis of the materials at different stages of the synthesis process were demonstrated in Figure 4. It was not difficult to find that the ζ potential value presented a decline after the essential oils were loaded, without exception, which was attributed to the surface charge of capsaicin being negative [57]. In addition, the bare MCM-41 maintained a negative ζ value, which was ascribed to the deprotonated silanol groups attached to its surface [58]. MCM-41 changed the negative charge into the opposite after the successful functionalization of the amino group. Moreover, the Zein heightened the ζ potential values after being attached to the bare material. According to the changes of electric charge among different materials, electrostatic attraction could be considered as one of the reasons for the improvement of antibacterial ability [59].

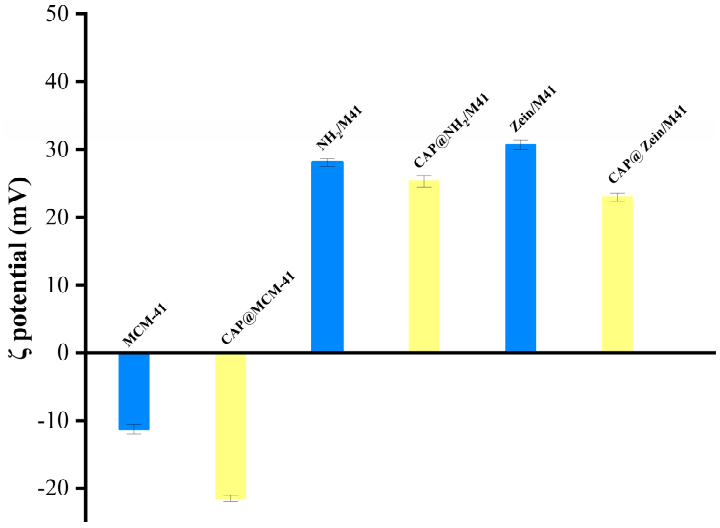

Figure 4. ζ potential values of the bacteriostatic agent in different synthesis steps.

3.1.5. Nitrogen Adsorption/Desorption

To investigate the specific surface area, nitrogen sorption isotherm measurements were conducted at 77 K. Nitrogen sorption isotherm curves of MCM-41 presented typical type IV behavior (Figure 5), which was characteristic of mesoporous materials [60]. The BET surface areas were evaluated to be as high as 636.68 $m^2 \cdot g^{-1}$ for MCM-41 (Table 1). Notably, the high BET surface area of MCM-41 was good for improving the load rate [61]. The average diameter of pores of MCM-41 was 2.78 nm, which was consistent with the theoretical pore size of malodorous distribution. Figure 5 showed the nitrogen adsorption-desorption isotherms with hysteresis of type IV behavior, indicating the mesoporous structure of NH_2/M41 with a higher value of pore diameter. The calculated BET surface area of NH_2/M41 was 368.26 $m^2 \cdot g^{-1}$. These results were in good agreement with the results of other studies [62]. A significant decrease in the BET surface area and pore volume was observed for the amino-modified MCM-41, which indicated that NH_2/M41 was successfully prepared and that its condensation degree of silanol groups differed from bare MCM-41. The nitrogen adsorption-desorption isotherm and corresponding pore size value were carried out to confirm the mesoporous nature of the Zein/M41. The lowest pore diameter value of Zein/M41 demonstrated that the pores on the bare materials had been packaged, further confirming the coexistence of Zein in the material [63]. However, the surface area of Zein/M41 continued to decrease to 290.32 $m^2 \cdot g^{-1}$, lower than that of previously reported ordered NH_2/M41, as showed in Table 1, indicating that the NH_2/M41 was filled by or covered with the pore space of Zein. It was clearly evident that by modification, the surface area of NH_2/M41 decreased, which could be attributed to the addition of Zein [64].

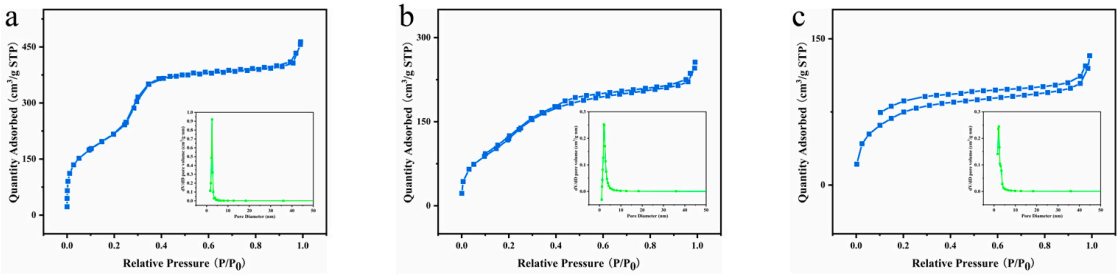

Figure 5. N_2 adsorption/desorption isotherms and pore size distributions of (**a**) MCM-41; (**b**) NH_2/M41 and (**c**) Zein/M41.

Table 1. Surface characteristics of CAP@ Zein/M41 matrix in different synthesis steps.

Nanoparticles	Specific Surface Area (m^2/g)	Pore Volume (cm^3/g)	Pore Size (nm)
MCM-41	636.68	0.7121	4.2736
NH_2/M41	368.26	0.3931	4.4693
Zein/M41	290.32	0.3898	5.3706

3.2. Sustained Release Test

In order to further explore the features of MSNs, a molecular gate was introduced on behalf of meeting diverse requirements of the multi-responsive controlled release, which has promising biological applications [65]. Traditionally, a self-immolating gate has been one of the molecular gate forms, which applied to dye-loaded silica mesoporous nanoparticles. Once the solution turned alkaline, the gate would disappear and turn into emancipated dye. In other words, the gate remains closed, leading to low levels of dye release at acidic and neutral pH, which could be called a pH-response. Despite the pH-response being the most common response in previous research, enzyme-response was another prevalent method for controlled release of EOs or other effective constituents. Researchers have described a new gated nanodevice design that uses glucose as a trigger and cyclodextrin-modified glucose oxidase as a capping agent to control cargo delivery. In this study, Zein is one kind of nitrogen source during the bacterial growth process, and could be consumed by *E. coli* and *S. aureus*, permitting capsaicin to be sent out. The enzyme generated by the bacterium was the trigger for dissolving Zein in the surface layer of the antibacterial agent.

Essential oil release experiments were performed to detect the controlled release capacity of CAP@ Zein/M41 by comparison [66]. Release rates of two kinds of materials in different simulated solutions are all shown in Figure 6 [67]. It is worth noting that the release rate of CAP@ Zein/M41 remained at a very low value for the whole period, when it was vibrated in single TSB solution without bacteria solution added (Figure 6a). CAP@MCM-41 was designed as the control group to confirm that CAP@ Zein/M41 possessed good stability, because CAP@MCM-41 presented burst release behavior even though it was in single TSB solution (Figure 6c), just a little bit slower than in TSB solution with *E. coli* (10^6 CFU/mL) (Figure 6d). CAP@ Zein/M41, under the environment of solution with *E. coli* (10^6 CFU/mL), presented the ability of controlled release of essential oils (Figure 6b). CAP@MCM-41 began releasing capsaicin immediately when it got to the solution, especially in the first several hours, where the loss rate increased up to 75.09% (Figure 6b). Furthermore, the release percent of capsaicin at CAP@MCM-41 reached 81.56% as the maximum value. In contrast with CAP@MCM-41, CAP@ Zein/M41 exhibited superior stability in the controlled release aspect, which was in accordance with the previous study [37]. Although in full contact with the bacteria, CAP@ Zein/M41 remained unchanged in the initial stage, then was abruptly released from Zein/M41. Finally, the CAP@ Zein/M41 resolved slowly at a mild rate until meeting the peak. This validated that the delivery of encapsulated capsaicin was hampered by the Zein grafted onto the MSNs, and the existence of *E. coli* and *S. aureus* made for the release of the encapsulated cargo. Zein was hydrolyzed by the secretions of bacteria, resulting in the controlled release of the entrapped capsaicin. Thus, the release pattern also conformed to the growth curve of *E. coli* and *S. aureus*.

3.3. Antibacterial Performance

EOs are famous for their superior antimicrobial effects, and silica nanocapsules are equipped with a high loading capacity of EOs. Hence, they are appropriate for creating environmentally friendly bacteriostatic agents. Further, MCM-41 improved the antibacterial efficiency of capsaicin, considering the MIC value.

The antimicrobial efficacy of free capsaicin and CAP@ Zein/M41 was assessed by the minimal bactericidal concentration (MBC) using broth macroevolution methods [68]. The growth reduction value demonstrated that the capsaicin had a broad spectrum of antibacterial inhibition. Furthermore, the MBC counted for 1–2 mg/mL against a Gram-positive

bacterium and 2–4 mg/mL against a Gram-negative bacterium, respectively (Figure 7). CAP@Zein/M41, the end product after encapsulating the essential oils, presented a different degree of antibacterial effect regarding its concentration in the initial stages. Additionally, the MBC of both the Gram-positive bacterium and Gram-negative one was determined to be 1.5 mg/mL. These data implied that the antibacterial activity of capsaicin was mounted after several functionalization procedures. Such a phenomenon could be attributed to the encapsulation of capsaicin on the surface and interior of the mesoporous silica nanoparticles. The result agreed with former research [69]. In addition, bare supports with the same concentration were also detected in the experiment to exclude the influence of the particles on the microorganism's survival. Non-functionalized materials had little inhibitory effect on the bacterium growth on account of the spread plate count results. This behavior agreed with previously reported results [70]. The growth curves of *E. coli* were presented in Figure 8, depicting the growth conditions under MIC and half of the MIC value. Further, it could be concluded that capsaicin not only presented a good inhibitory effect when encapsulated in gated MCM-41, but also demonstrated the improvement of its bactericidal effect by contrast with free EOs. Associated with the sustained release curve, it could be inferred that the growth of bacteria was actually linked with the amount of Zein in CAP@ Zein/M41. The results indicated that the bacteriostatic efficacy in the encapsulated form increased up to triple, by comparing with pure EOs [71]. Another piece of research demonstrated that combining eugenol and vanillin with silica microparticles as a novel fungistat reduced the microbial content by more than $5^{-\log}$ [72].

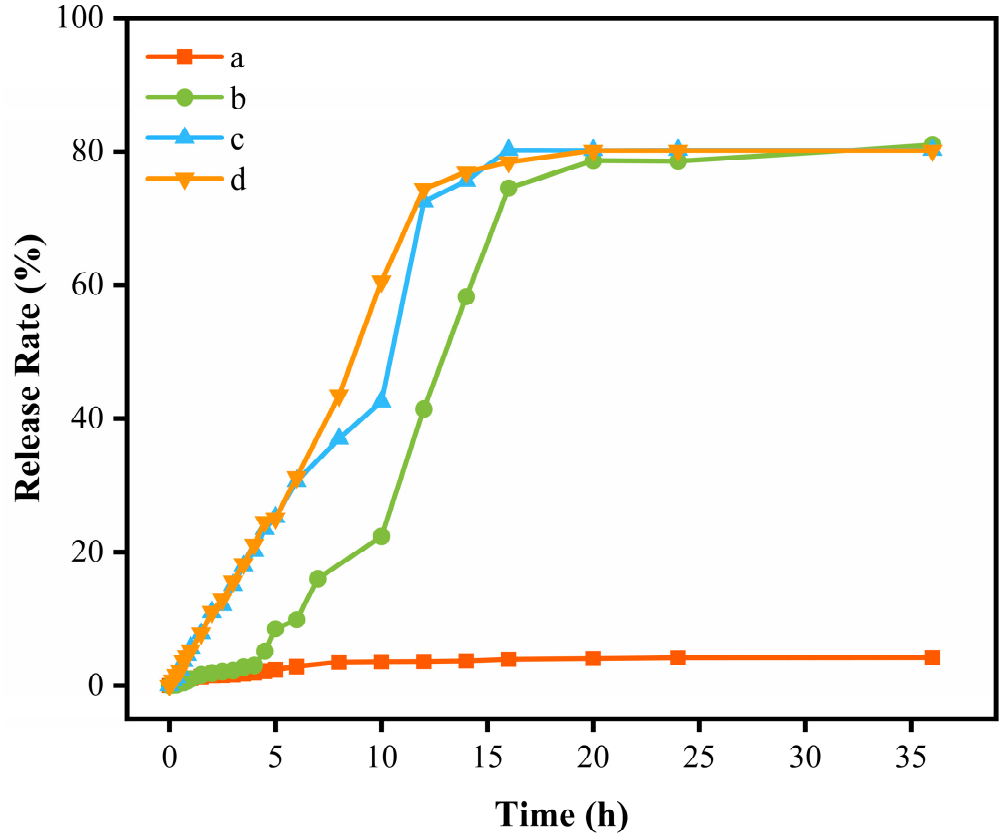

Figure 6. Sustained release profiles of capsaicin loaded in: (**a**) CAP@ Zein/M41 in pure TSB solution; (**b**) CAP@ Zein/M41 in TSB solution with *E. coli* (10^6 CFU/mL); (**c**) CAP@MCM-41 in pure TSB solution; (**d**) CAP@MCM-41 in TSB solution with *E. coli* (10^6 CFU/mL).

3.4. Antibacterial Mechanism

After being exposed to CAP@ Zein/M41, the FE-SEM observations of the bacterial cell morphology allowed researchers to investigate the antibacterial mechanism and assess the antibacterial effectiveness. Figure 9 displayed the outcomes of bacterial cells that revealed

the severity and nature of cell damage. The natural strains of *S. aureus* and *E. coli* had the characteristic globular and rod shapes, respectively. The electron micrographs (Figure 9) told us that there was a clear change in the surface morphology of *E. coli* cells after dealing with CAP@ Zein/M41. After being exposed to CAP@ Zein/M41, the bacteria cell bodies of *E. coli* and *S. aureus* were badly damaged, such as shrinking, perforating, breaking, and bursting. The possible action mechanism of the antibacterial activity by capsaicin against *E. coli* and *S. aureus* is depicted in Figure 10.

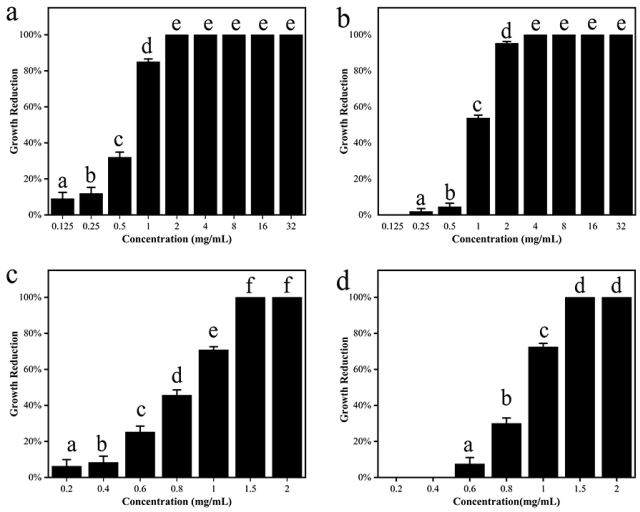

Figure 7. The growth reduction of (**a**) *E. coli* and (**b**) *S. aureus* treated with capsaicin at 24 h; the growth reduction of (**c**) *E. coli* and (**d**) *S. aureus* treated with CAP@ Zein/M41 at 24 h. The same letters in the bars show homogeneous group membership ($p < 0.05$) (n = 3).

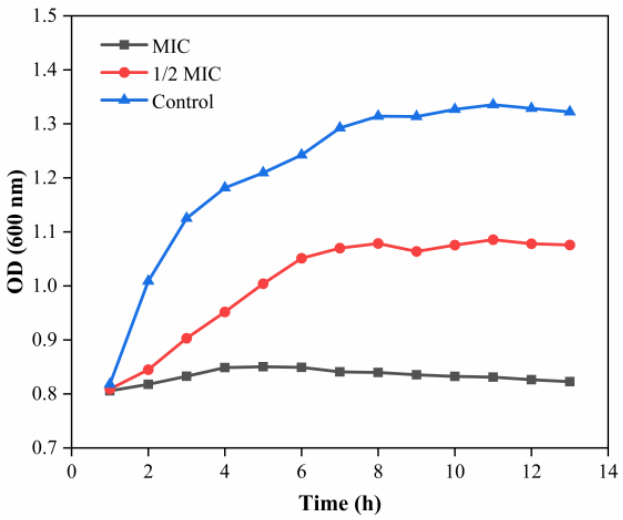

Figure 8. The growth curve of *E. coli* with different concentrations of capsaicin.

Briefly, with the enzyme-response molecular gate, we designed the "essential oil-controlled-gating" strategy for mesoporous silica antibacterial materials. Since traditional encapsulation presented a poor ability in avoiding the volatility of EOs, a molecular gate made by Zein was applied in this novel antimicrobial carrier, where capsaicin played the role of an effective constituent in bacteriostatic activity, MCM-41 acted as the basic vector, and Zein was regarded as the enzyme-response molecular gate. As can be seen from the above characterization, this bacteriostatic material not only further upgraded the stability and utilization rate of bacteriostatic drugs, but also attracted more bacteria with its unique structure and surface charge. In comparison with capsaicin-functionalized MCM-41, CAP@ Zein/M41 possessed a higher load rate, which can be more economic and

efficient, further lowering the degree of risk. The bacteriostatic results depicted that CAP@ Zein/M41 successfully enhanced the bacteriostatic activity of capsaicin in bacteria, which confirmed the success of the bacteriostatic material study. It is feasible to control the EOs' release from the Zein molecular gate, according to the sustain-release result.

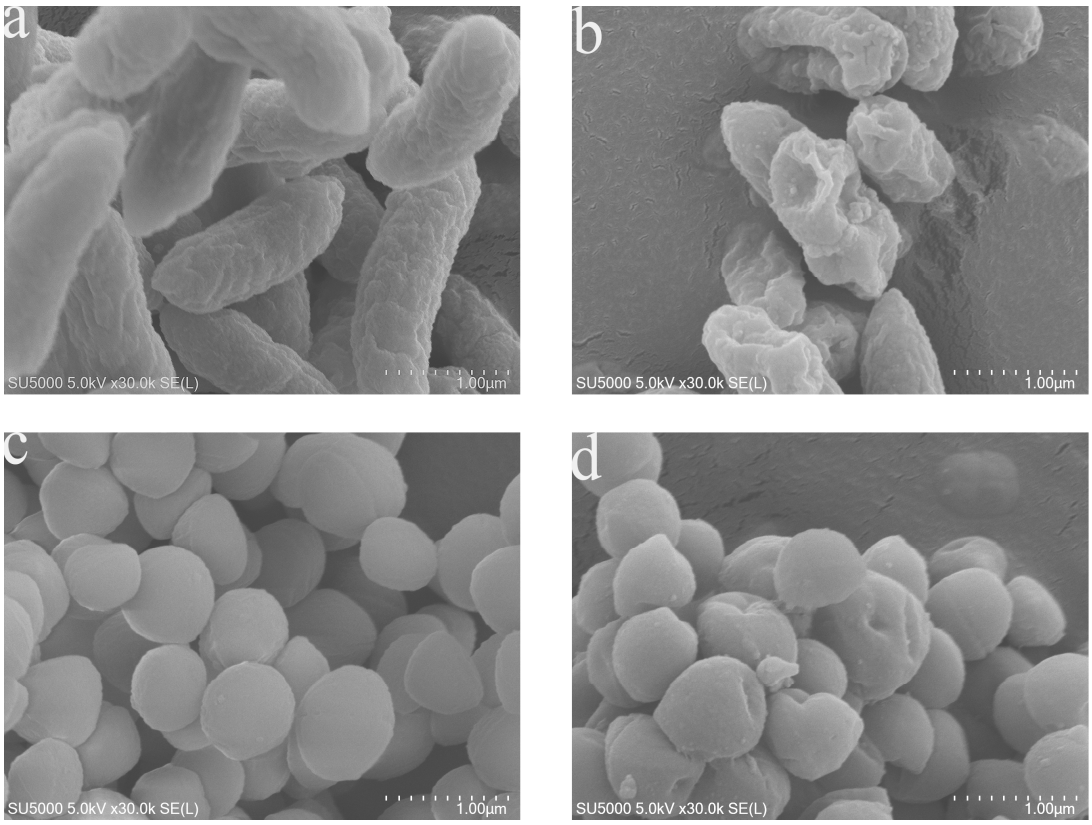

Figure 9. SEM images of (**a**) *E. coil* untreated; (**b**) *E. coli* treated with 3.0 mg/mL of CAP@ Zein/M41; (**c**) *S. aureus* untreated; (**d**) *S. aureus* treated with 3.0 mg/mL of CAP@ Zein/M41.

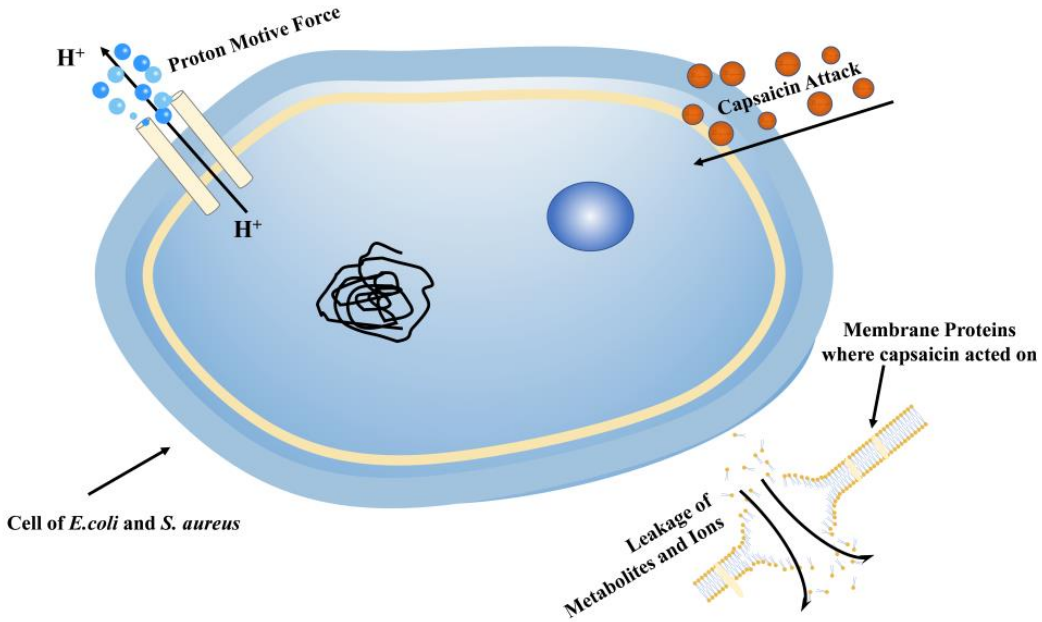

Figure 10. The schematic mechanism of the action (the antibacterial activity by capsaicin against *E. coli* and *S. aureus*).

4. Conclusions

A combination of mesoporous silica nanoparticles (MCM-41) after amino-functionalization and capsaicin was applied to construct slow-release nanoparticles (CAP@MCM-41), and Zein was utilized as the molecular gate to show controlled release. The results of this study demonstrated that the cooperation of Zein and CAP@MCM-41 could better enhance the antibacterial activity of the materials and extend the service life of this novel bacteriostatic agent through designing the molecular gate and creating the controlled release. Particularly, the MBC of CAP@ Zein/M41 was 1–1.5 mg/mL, and the efficiency of drug release was higher than 80%, which was calculated with the load rate. SEM showed that the surface of CAP@ Zein/M41 was relatively smooth, and the morphology hardly changed, proving that CAP@ Zein/M41 had good interface compatibility. Moreover, ζ potential analysis depicted that amino-functionalization influenced the surface charge of bare MCM-41, increasing the appeal of bacteria. The addition of Zein had little impact on the ζ potential value. Therefore, CAP@MCM-41 laid a better foundation for preparing the controlled release antibacterial materials in the food conservation area. Multiple responsive elements were vital for the controlled release, including protease, redox, and pH [73]. The application of molecular-gate materials in food antibacterial agents and food preservation has attracted increasing attention in recent years thanks to the controlled release ability of essential oils or other useful antibacterial components based on the use of external stimuli.

Author Contributions: Conceptualization, Y.S.; methodology, Y.S. and J.S.; software, H.S. and Y.L.; validation, J.S. and Y.S.; formal analysis, H.S.; investigation, H.S. and Y.L.; resources, Y.S.; data curation, H.S. and Y.L.; writing—original draft preparation, H.S.; writing—review and editing, J.S. and Y.S.; visualization, H.S. and Y.L.; supervision, J.S. and Y.S.; project administration, J.S. and Y.S.; funding acquisition, Y.S. All authors have read and agreed to the published version of the manuscript.

Funding: This research was funded by the National Natural Science Foundation of China (32272399).

Institutional Review Board Statement: Not applicable.

Informed Consent Statement: Not applicable.

Data Availability Statement: The data presented in this study are available on request from the corresponding author.

Conflicts of Interest: The authors declare no conflict of interest.

References

1. Liu, F.; Saricaoglu, F.T.; Avena-Bustillos, R.J.; Bridges, D.F.; Takeoka, G.R.; Wu, V.; Chiou, B.S.; Wood, D.F.; Mchugh, T.H. Preparation of fish skin gelatin-based nanofibers incorporating cinnamaldehyde by solution blow spinning 4. *Int. J. Mol. Sci.* **2019**, *19*, 618. [CrossRef] [PubMed]
2. Andriotis, E.G.; Papi, R.M.; Paraskevopoulou, A.; Achilias, D.S. Synthesis of D-Limonene loaded polymeric nanoparticles with enhanced antimicrobial properties for potential application in food packaging. *Nanomaterials* **2021**, *11*, 191. [CrossRef] [PubMed]
3. Li, Y.M.; Huang, T.Y.; Mao, Y.Z.; Chen, Y.N.; Shi, F.; Peng, R.X.; Chen, J.X.; Yuan, L.; Bai, C.Y.; Chen, L.; et al. Study on the viable but non-culturable (VBNC) state formation of staphylococcus aureus and its control in food system. *Front. Microbiol.* **2020**, *11*, 599739. [CrossRef] [PubMed]
4. Wang, H.H.; Huang, M.Y.; Zeng, X.M.; Peng, B.; Xu, X.L.; Zhou, G.H. Resistance profiles of salmonella isolates exposed to stresses and the expression of small non-coding RNAs. *Front. Microbiol.* **2020**, *11*, 130. [CrossRef] [PubMed]
5. Paden, H.; Ilic, S.; Hatsu, I.; Kane, K.; Lustberg, M.; Grenade, C.; Bhatt, A.; Pardo, D.D.; Beery, A. Assessment of food safety knowledge and behaviors of cancer patients receiving treatment. *J. Acad. Nutr. Diet.* **2020**, *120*, A46. [CrossRef]
6. Onyebuchi, C.; Kavaz, D. Chitosan and N, N, N-Trimethyl chitosan nanoparticle encapsulation Of ocimum gratissimum essential oil: Optimised synthesis, in vitro release And bioactivity. *Int. J. Nanomed.* **2019**, *14*, 7707–7727. [CrossRef]
7. Lien, K.W.; Yang, M.X.; Ling, M.P. Microbial risk assessment of escherichia coli O157:H7 in beef imported from the United States of America to Taiwan. *Microorganisms* **2020**, *8*, 676. [CrossRef]
8. Jaiswal, S. Salmonella, Food safety and food handling practices. *Foods* **2021**, *10*, 907.
9. Qian, X.; Yanagi, K.; Kane, A.V.; Alden, N.; Lei, M.; Snydman, D.R.; Vickers, R.J.; Lee, K.; Thorpe, C.M. Ridinilazole, a narrow spectrum antibiotic for treatment of clostridioides difficile infection, enhances preservation of microbiota-dependent bile acids. *Am. J. Physiol.-Gastrointest. Liver Physiol.* **2020**, *319*, G227–G237. [CrossRef]

10. Carlson, T.J.; Gonzales-Luna, A.J.; Garey, K.W. Recent developments in antimicrobial therapy for gastrointestinal infections. *Curr. Opin. Gastroenterol.* **2021**, *37*, 30–36. [CrossRef]
11. Schlattmann, A.; Lützau, K.; Kaspar, U.; Becker, K. The porcine nasal microbiota with particular attention to livestock-associated methicillin-resistant staphylococcus aureus in Germany—A culturomic approach. *Microorganisms* **2020**, *8*, 514. [CrossRef] [PubMed]
12. Rudramurthy, G.R.; Swamy, M.K.; Sinniah, U.R.; Ghasemzadeh, A. Nanoparticles: Alternatives against drug-resistant pathogenic microbes. *Molecules* **2016**, *21*, 836. [CrossRef] [PubMed]
13. Saleh, I.; Abu-Dieyeh, M.H. Novel Prosopis juliflora leaf ethanolic extract as natural antimicrobial agent against food spoiling microorganisms. *Sci. Rep.* **2021**, *11*, 7871. [CrossRef] [PubMed]
14. Abu Ali, O.A.; El-Naggar, M.E.; Abdel-Aziz, M.S.; Saleh, D.I.; Abu-Saied, M.A.; El-Sayed, W.A. Facile synthesis of natural anise-based nanoemulsions and their antimicrobial activity. *Polymers* **2021**, *13*, 2009. [CrossRef] [PubMed]
15. Zhang, T.; Luo, Y.; Wang, M.X.; Chen, F.; Liu, J.K.; Meng, K.; Zhao, H.J. Double-layered microcapsules significantly improve the long-term effectiveness of essential oil. *Polymers* **2020**, *12*, 1651. [CrossRef]
16. Wiatrak, K.; Morawiec, T.; Roj, R.; Kownacki, P.; Nitecka-Buchta, A.; Niedzielski, D.; Wychowanski, P.; Machorowska-Pieniazek, A.; Cholewka, A.; Baldi, D.; et al. Evaluation of Effectiveness of a Toothpaste Containing tea tree oil and ethanolic extract of propolis on the improvement of oral health in patients using removable partial dentures. *Molecules* **2021**, *26*, 4071. [CrossRef]
17. Valkova, V.; Duranova, H.; Galovicova, L.; Vukovic, N.L.; Vukic, M.; Kacaniova, M. In vitro antimicrobial activity of lavender, mint, and rosemary essential oils and the effect of their vapours on growth of penicillium spp. in a bread model system. *Molecules* **2021**, *26*, 3859. [CrossRef]
18. Muta, T.; Parikh, A.; Kathawala, K.; Haidari, H.; Song, Y.M.; Thomas, J.; Garg, S. Quality-by-Design approach for the development of nano-sized tea tree oil formulation-impregnated biocompatible gel with antimicrobial properties. *Pharmaceutics* **2020**, *12*, 1091. [CrossRef]
19. Partheniadis, I.; Zarafidou, E.; Litinas, K.E.; Nikolakakis, I. Enteric Release Essential Oil Prepared by co-spray drying methacrylate/polysaccharides-influence of starch type. *Pharmaceutics* **2020**, *12*, 571. [CrossRef]
20. Yong, G.R.; Gebru, Y.A.; Kim, D.W.; Kim, D.H.; Han, H.A.; Kim, Y.H.; Kim, M.K. Chemical composition and antioxidant activity of steam-distilled essential oil and glycosidically bound volatiles from maclura tricuspidata fruit. *Foods* **2019**, *8*, 659. [CrossRef]
21. Kuzma, M.; Fodor, K.; Almasi, A.; Mozsik, G.; Past, T.; Perjesi, P. Toxicokinetic study of a gastroprotective dose of capsaicin by HPLC-FLD method. *Molecules* **2019**, *24*, 2848. [CrossRef]
22. Kursunluoglu, G.; Taskiran, D.; Kayali, H.A. The investigation of the antitumor agent toxicity and capsaicin effect on the electron transport chain enzymes, catalase activities and lipid peroxidation levels in lung, heart and brain tissues of rats. *Molecules* **2018**, *23*, 3267. [CrossRef] [PubMed]
23. Barbosa, S.; Saurina, J.; Puignou, L.; Nunez, O. Targeted UHPLC-HRMS (Orbitrap) polyphenolic and capsaicinoid profiling for the chemometric characterization and classification of paprika with protected designation of origin (PDO) attributes. *Molecules* **2020**, *25*, 1623. [CrossRef]
24. Iturrioz-Rodriguez, N.; Correa-Duarte, M.A.; Valiente, R.; Fanarraga, M.L. Engineering sub-cellular targeting strategies to enhance safe cytosolic silica particle dissolution in cells. *Pharmaceutics* **2020**, *12*, 487. [CrossRef]
25. Jin, L.; Huang, Q.J.; Zeng, H.Y.; Du, J.Z.; Xu, S.; Chen, C.R. Hydrotalcite-gated hollow mesoporous silica delivery system for controlled drug release. *Microporous Mesoporous Mater.* **2019**, *274*, 304–312. [CrossRef]
26. Liu, Y.H.; Jin, L.; Wang, C.; Sheng, J.; Song, Y.S. Thymol-functionalized hollow mesoporous silica spheres nanoparticles: Preparation, characterization and bactericidal activity. *Bull. Mater. Sci.* **2021**, *44*, 126. [CrossRef]
27. Raja, R.K.; Nguyen-Tri, P.; Balasubramani, G.; Alagarsamy, A.; Hazir, S.; Ladhari, S.; Saidi, A.; Pugazhendhi, A.; Samy, A.A. SARS-CoV-2 and its new variants: A comprehensive review on nanotechnological application insights into potential approaches. *Appl. Nanosci.* **2021**. [CrossRef]
28. Lesniewska, B.; Arciszewska, Z.; Wawrzynczak, A.; Jarmolinska, S.; Nowak, I.; Godlewska-Zylkiewicz, B. Method development for determination of trace amounts of palladium in environmental water samples by ICP-MS/MS after pre-concentration on thiol-functionalized MCM-41 materials. *Talanta* **2020**, *217*, 121004. [CrossRef]
29. Ozcelik, N.; Yurtcan, A.B. Drug loading with supercritical carbon dioxide deposition on different silica derivatives: Carvedilol study. *J. Drug Deliv. Sci. Technol.* **2019**, *53*, 101213. [CrossRef]
30. Jin, L.; Teng, J.; Hu, L.H.; Lan, X.T.; Xu, Y.; Sheng, J.; Song, Y.S.; Wang, M.F. Pepper fragrant essential oil (PFEO) and functionalized MCM-41 nanoparticles: Formation, characterization, and bactericidal activity. *J. Sci. Food Agric.* **2019**, *99*, 5168–5175. [CrossRef]
31. Yang, B.Y.; Dong, Y.X.; Wang, F.; Zhang, Y. Nanoformulations to enhance the bioavailability and physiological functions of polyphenols. *Molecules* **2020**, *25*, 4613. [CrossRef] [PubMed]
32. Martinez-Edo, G.; Llinas, M.C.; Borros, S.; Sanchez-Garcia, D. Isothiocyanate-Functionalized mesoporous silica nanoparticles as building blocks for the design of nanovehicles with optimized drug release profile. *Nanomaterials* **2019**, *9*, 1219. [CrossRef] [PubMed]
33. Kumar, P.; Pahal, V.; Gupta, A.; Vadhan, R.; Chandra, H.; Dubey, R.C. Effect of silver nanoparticles and Bacillus cereus LPR2 on the growth of Zea mays. *Sci. Rep.* **2020**, *10*, 20409. [CrossRef]
34. Tomsone, L.; Galoburda, R.; Kruma, Z.; Durrieu, V.; Cinkmanis, I. Microencapsulation of horseradish (*Armoracia rusticana* L.) juice using spray-drying. *Foods* **2020**, *9*, 1332. [CrossRef] [PubMed]

35. Hou, J.J.; Weng, R.Y.; Jiang, W.W.; Sun, H.M.; Xia, J.T.; Liu, Y.T.; Sheng, J.; Song, Y.S. In-situ preparation of novel sedimentary rock-like Fe_3O_4 by rice-husk mesoporous silica as templates for effective remove As(III) from aqueous solutions. *J. Environ. Chem. Eng.* **2021**, *9*, 105866. [CrossRef]
36. Hou, J.J.; Xia, J.T.; Weng, R.Y.; Liu, Y.T.; Li, L.Y.; Liu, K.Y.; Sheng, J.; Song, Y.S. Mesoporous silicon extracted from rice husk for remediation of different sorts of dyestuffs from simulated textile effluent: Kinetic, isotherm, and mechanism study. *Biomass Convers. Biorefin.* **2022**. [CrossRef]
37. Gao, F.; Zhou, H.J.; Shen, Z.C.; Zhu, G.W.; Hao, L.; Chen, H.Y.; Xu, H.; Zhou, X.H. Long-lasting anti-bacterial activity and bacteriostatic mechanism of tea tree oil adsorbed on the amino-functionalized mesoporous silica-coated by PAA. *Colloids Surf. B Biointerfaces* **2020**, *188*, 110784. [CrossRef]
38. Sanchez-Arreguin, A.; Carriles, R.; Ochoa-Alejo, N.; Lopez, M.G.; Sanchez-Segura, L. Generation of BSA-capsaicin nanoparticles and their hormesis effect on the rhodotorula mucilaginosa yeast. *Molecules* **2019**, *24*, 2800. [CrossRef]
39. Chamignon, C.; Gueneau, V.; Medina, S.; Deschamps, J.; Gil-Izquierdo, A.; Briandet, R.; Mousset, P.Y.; Langella, P.; Lafay, S.; Bermudez-Humaran, L.G. Evaluation of the probiotic properties and the capacity to form biofilms of variouslactobacillusstrains. *Microorganisms* **2020**, *8*, 1053. [CrossRef]
40. Singh, P.; Pandit, S.; Mokkapati, V.; Garnaes, J.; Mijakovic, I. A sustainable approach for the green synthesis of silver nanoparticles fromsolibacillus isronensissp. and their application in biofilm inhibition. *Molecules* **2020**, *25*, 2783. [CrossRef]
41. Chanaj-Kaczmarek, J.; Paczkowska, M.; Osmalek, T.; Kapron, B.; Plech, T.; Szymanowska, D.; Karazniewicz-Lada, M.; Kobus-Cisowska, J.; Cielecka-Piontek, J. Hydrogel delivery system containingcalendulae floslyophilized extract with chitosan as a supporting strategy for wound healing applications. *Pharmaceutics* **2020**, *12*, 634. [CrossRef] [PubMed]
42. Leclercq, L.; Nardello-Rataj, V. How to improve the chemical disinfection of contaminated surfaces by viruses, bacteria and fungus? *Eur. J. Pharm. Sci.* **2020**, *155*, 105559. [CrossRef] [PubMed]
43. Guo, N.; Gai, Q.Y.; Jiao, J.; Wang, W.; Zu, Y.G.; Fu, Y.J. Antibacterial activity of fructus forsythia essential oil and the application of EO-loaded nanoparticles to food-borne pathogens. *Foods* **2016**, *5*, 73. [CrossRef]
44. Ribes, S.; Ruiz-Rico, M.; Perez-Esteve, E.; Fuentes, A.; Talens, P.; Martinez-Manez, R.; Barat, J.M. Eugenol and thymol immobilised on mesoporous silica-based material as an innovative antifungal system: Application in strawberry jam. *Food Control* **2017**, *81*, 181–188. [CrossRef]
45. Shi, F.; Wu, J.C.; Zhao, Y.; Zhao, B.; Kong, X.T. Controllable assembly and application of janus smart nanosheets for oil displacement. *Front. Chem.* **2020**, *8*, 154. [CrossRef] [PubMed]
46. Suttiruengwong, S.; Pivsa-Art, S.; Chareonpanich, M. Hydrophilic and hydrophobic mesoporous silica derived from rice husk ash as a potential drug carrier. *Materials* **2018**, *11*, 1142. [CrossRef]
47. Liu, Q.D.; He, P.L.; Yu, H.D.; Gu, L.; Ni, B.; Wang, D.; Wang, X. Single molecule-mediated assembly of polyoxometalate single-cluster rings and their three-dimensional superstructures. *Sci. Adv.* **2019**, *5*, eaax1081. [CrossRef]
48. Tong, Z.W.; Gul, H.; Awais, M.; Saddick, S.; Khan, F.S.; Gulfraz, M.; Afzal, U.; Nazir, K.; Malik, M.Y.; Khan, S.U.; et al. Determination of in vivo biological activities of Dodonaea viscosa flowers against CCL4 toxicity in albino mice with bioactive compound detection. *Sci. Rep.* **2021**, *11*, 13336. [CrossRef]
49. Akhmetova, A.; Lanno, G.M.; Kogermann, K.; Malmsten, M.; Rades, T.; Heinz, A. Highly elastic and water stable zein microfibers as a potential drug delivery system for wound healing. *Pharmaceutics* **2020**, *12*, 458. [CrossRef]
50. Boateng-Marfo, Y.; Dong, Y.C.; Ng, W.K.; Lin, H.S. Artemether-loaded zein nanoparticles: An innovative intravenous dosage form for the management of severe malaria. *Int. J. Mol. Sci.* **2021**, *22*, 1141. [CrossRef]
51. Esposito, D.; Dal Poggetto, G.; Demont, A.; Kraut, N.; Miro, A.; Ungaro, F.; Laurienzo, P.; Quaglia, F. Zein Beta-cyclodextrin micropowders for iron bisglycinate delivery. *Pharmaceutics* **2020**, *12*, 60. [CrossRef] [PubMed]
52. Wu, Z.Y.; Chen, M.X.; Chu, S.Q.; Lin, Y.; Liang, H.W.; Zhang, J.; Yu, S.H. Switching Co/N/C catalysts for heterogeneous catalysis and electrocatalysis by controllable pyrolysis of cobalt porphyrin. *Iscience* **2019**, *15*, 282–290. [CrossRef] [PubMed]
53. Uemura, T.; Kaseda, T.; Sasaki, Y.; Inukai, M.; Toriyama, T.; Takahara, A.; Jinnai, H.; Kitagawa, S. Mixing of immiscible polymers using nanoporous coordination templates. *Nat. Commun.* **2015**, *6*, 7473. [CrossRef] [PubMed]
54. Rotjanasuworapong, K.; Lerdwijitjarud, W.; Sirivat, A. Synthesis and Characterization of $Fe_{0.8}Mn_{0.2}Fe_2O_4$ Ferrite Nanoparticle with high saturation magnetization via the surfactant assisted co-precipitation. *Nanomaterials* **2021**, *11*, 876. [CrossRef] [PubMed]
55. Juarez, L.A.; Anon, E.; Gimenez, C.; Sancenon, F.; Martinez-Manez, R.; Costero, A.M.; Gavina, P.; Parra, M.; Bernardos, A. Self-immolative linkers as caps for the design of gated silica mesoporous supports. *Chem.—Eur. J.* **2016**, *22*, 14126–14130. [CrossRef]
56. Aznar, E.; Villalonga, R.; Gimenez, C.; Sancenon, F.; Marcos, M.D.; Martinez-Manez, R.; Diez, P.; Pingarron, J.M.; Amoros, P. Glucose-triggered release using enzyme-gated mesoporous silica nanoparticles. *Chem. Commun.* **2013**, *49*, 6391–6393. [CrossRef]
57. Yuan, Y.; Liu, Y.; He, Y.; Zhang, B.K.; Zhao, L.; Tian, S.M.; Wang, Q.M.; Chen, S.A.; Li, Z.K.; Liang, S.; et al. Intestinal-targeted nanotubes-in-microgels composite carriers for capsaicin delivery and their effect for alleviation of Salmonella induced enteritis. *Biomaterials* **2022**, *287*, 121613. [CrossRef]
58. Rakhshaei, R.; Namazi, H. A potential bioactive wound dressing based on carboxymethyl cellulose/ZnO impregnated MCM-41 nanocomposite hydrogel. *Mater. Sci. Eng. C Mater. Biol. Appl.* **2017**, *73*, 456–464. [CrossRef]

59. Poyatos-Racionero, E.; Guari-Borras, G.; Ruiz-Rico, M.; Morella-Aucejo, A.; Aznar, E.; Barat, J.M.; Martinez-Manez, R.; Marcos, M.D.; Bernardos, A. Towards the enhancement of essential oil components' antimicrobial activity using new zein protein-gated mesoporous silica microdevices. *Int. J. Mol. Sci.* **2021**, *22*, 3795. [CrossRef]
60. Feng, X.; Ding, X.S.; Chen, L.; Wu, Y.; Liu, L.L.; Addicoat, M.; Irle, S.; Dong, Y.P.; Jiang, D.L. Two-dimensional artificial light-harvesting antennae with predesigned high-order structure and robust photosensitising activity. *Sci. Rep.* **2016**, *6*, 32944. [CrossRef]
61. Qu, Q.; Zhang, J.H.; Wang, J.; Li, Q.Y.; Xu, C.W.; Lu, X.H. Three-dimensional ordered mesoporous Co_3O_4 enhanced by Pd for oxygen evolution reaction. *Sci. Rep.* **2017**, *7*, 41542. [CrossRef] [PubMed]
62. Szegedi, A.; Popova, M.; Goshev, I.; Mihály, J. Effect of amine functionalization of spherical MCM-41 and SBA-15 on controlled drug release. *J. Solid State Chem.* **2011**, *184*, 1201–1207. [CrossRef]
63. Li, B.Y.; Yang, X.J.; Xia, L.L.; Majeed, M.I.; Tan, B. Hollow microporous organic capsules. *Sci. Rep.* **2013**, *3*, 2128. [CrossRef]
64. Pawar, R.C.; Kang, S.; Park, J.H.; Kim, J.H.; Ahn, S.; Lee, C.S. Room-temperature synthesis of nanoporous 1D microrods of graphitic carbon nitride (g-C_3N_4) with highly enhanced photocatalytic activity and stability. *Sci. Rep.* **2016**, *6*, 31147. [CrossRef]
65. Polo, L.; Gomez-Cerezo, N.; Garcia-Fernandez, A.; Aznar, E.; Vivancos, J.L.; Arcos, D.; Vallet-Regi, M.; Martinez-Manez, R. Mesoporous bioactive glasses equipped with stimuli-responsive molecular gates for controlled delivery of levofloxacin against bacteria. *Chem.—Eur. J.* **2018**, *24*, 18944–18951. [CrossRef] [PubMed]
66. Bhakta, H.C.; Lin, J.M.; Grover, W.H. Measuring dissolution profiles of single controlled-release drug pellets. *Sci. Rep.* **2020**, *10*, 19734. [CrossRef] [PubMed]
67. Lin, R.T.; Wang, Z.R.; Li, Z.H.; Gu, L.S. A two-phase and long-lasting multi-antibacterial coating enables titanium biomaterials to prevent implants-related infections. *Mater. Today Bio* **2022**, *15*, 100330. [CrossRef] [PubMed]
68. Wenting, L.; Siying, L.; Shiti, S.; Yuqing, Z.; Sameen, D.E.; Li, H.; Yaowen, L. Investigation of ultrasonic treatment on physico-chemical, structural and morphological properties of sodium alginate/AgNPs/apple polyphenol films and its preservation effect on strawberry. *Polymers* **2020**, *12*, 2096. [CrossRef]
69. Ruiz-Rico, M.; Perez-Esteve, E.; de la Torre, C.; Jimenez-Belenguer, A.I.; Quiles, A.; Marcos, M.D.; Martinez-Manez, R.; Barat, J.M. Improving the antimicrobial power of low-effective antimicrobial molecules through nanotechnology. *J. Food Sci.* **2018**, *83*, 2140–2147. [CrossRef]
70. Ruiz-Rico, M.; Moreno, Y.; Barat, J.M. In vitro antimicrobial activity of immobilised essential oil components against Helicobacter pylori. *World J. Microbiol. Biotechnol.* **2020**, *36*, 3. [CrossRef]
71. Pena-Gomez, N.; Ruiz-Rico, M.; Fernandez-Segovia, I.; Barat, J.M. Study of apple juice preservation by filtration through silica microparticles functionalised with essential oil components. *Food Control* **2019**, *106*, 106749. [CrossRef]
72. Zhou, S.W.; Du, X.Z.; Cui, F.B.; Zhang, X.F. Multi-responsive and logic controlled release of dnagated mesoporous silica vehicles functionalized with intercalators for multiple delivery. *Small* **2014**, *10*, 980–988. [CrossRef] [PubMed]
73. Qiu, L.; Zhang, W.R.; Wang, S.Y.; Zhang, X.; Zhao, Y.B.; Cao, L.Q.; Sun, L. Construction of multifunctional porous silica nanocarriers for pH/enzyme-responsive drug release. *Mater. Sci. Eng. C Mater. Biol. Appl.* **2017**, *81*, 485–491. [CrossRef] [PubMed]